Saturation Point and Phase Envelope Calculation for Reactive Systems Based on the RAND Formulation

Fernando de Azevedo Medeiros, Erling Halfdan Stenby, Wei Yan*

Center for Energy and Resources Engineering, Department of Chemistry, Technical University of Denmark, 2800 Kongens Lyngby, Denmark

Abstract

Analysis of multicomponent reactive systems requires reliable and accurate equilibrium calculation. There are many stoichiometric or non-stoichiometric methods to solve the flash-type calculations of a mixture in chemical and phase equilibrium. In contrast, there is a lack of robust and efficient methods for another important type of equilibrium calculation, the saturation point calculation or the calculation under the phase fraction specification (β-specification), for a reactive mixture. In this work, we developed RAND-based algorithms for calculating the saturation points and phase envelope of a reactive mixture. The RAND formulation is a non-stoichiometric approach recently extended to non-ideal mixtures for different flash specifications. We showed here how to modify the RAND-based flash formulation to solve the β-specification problems. We distinguished between two types of phase fraction, the one based on components and the one based on elements. They led to different constraint equations in the formulation. Furthermore, we introduced element-based partition coefficients, similar to the equilibrium ratios or K-factors used for non-reactive mixtures. Use of these new variables are essential to cross the critical point of a reactive mixture in the phase envelope construction. Since the formulation developed for reactive mixtures is general, it can also be reduced and used for the simpler non-reactive mixtures. We showed how the reduction could be made and how the reduced algorithm served as an alternative approach to the prevailing phase envelope algorithm of Michelsen. We illustrated the robustness and efficiency of the proposed algorithm using four examples: Pxy diagrams for CO_2-NaCl brine, a solid-liquid Txy diagram for $MgCl_2$-water, a PT phase envelope for a reactive mixture with the alkene hydration reaction, and a PT phase envelope for a non-reactive hydrocarbon mixture.

Keywords:
Reactive Phase Diagram, Saturation Point, Txy Diagram, Pxy Diagram, Chemical Reactions, Phase Envelope

1. Introduction

The determination of phase equilibrium behavior of systems involving chemical reactions is crucial to the understanding of many processes, both in nature and in industrial applications. Hence, a great variety of approaches for solving chemical and phase equilibrium (CPE) problems can be found in the mainstream literature of areas such as chemical engineering [1], materials science [2] and earth sciences [3, 4].

CPE calculations are a special type of phase equilibrium calculation, where reaction equilibria need to be considered. Phase equilibrium calculations can be generally split into three main types, according to their specifications [5]: flash specifications, phase-fraction specifications, and indirect specifications. Problems under flash specifications are the ones that can be cast as minimization problems, and that is because the specified variables of the problem correspond to the canonical independent variables of a thermodynamic potential, such as the TP-flash, in which temperature (T) and pressure (P) are the canonical independent variables of the Gibbs energy (G). Phase-fraction specifications correspond to specifying the mole number of a phase (β), and these calculations are also known as saturation point calculations. Indirect specifications, such as critical point

calculations, correspond neither to the first type nor to the second. With a few exceptions, the discussions on CPE calculations have been focused on flash specifications.

In this work, we focus on the development of a general methodology for saturation point calculations in reactive systems. Saturation point calculations are especially important in the construction of phase diagrams such as the Txy and the Pxy phase diagrams for binary mixtures, in which the compositions of two phases in equilibrium are plotted as a function of T or P, at constant P or T, respectively. The construction of phase envelopes in the PT diagram is also a major application of saturation algorithms, and the three types of diagrams mentioned play a central role in areas such as process design [6, 7] and flow assurance [8].

The approach we have developed is based on the RAND method for solving CPE problems subject to phase fraction specifications, and is henceforth called saturation RAND. The RAND method was originally developed for flash specification problems in reactive systems, initially for TP-flash problems in ideal mixtures [9, 10] and later for non-ideal ones [11]. A new version of the RAND method, called modified RAND, has been developed [12] and applied to CPE problems under many different types of specifications to model mixtures of varying natures, such as hydrocarbon mixtures [13] and electrolytic solutions [14]. Despite the large number of specifications to which the modified RAND has been applied [15, 16], the problems

*Corresponding author
Email address:* weya@kemi.dtu.dk (Wei Yan)

have, until now, only involved flash specifications.

In the following sections, we first show the mathematical derivation of the saturation RAND formulation. The formulation is applied to a single-point calculation at a constant phase fraction. We further extend the formulation to construction of a PT phase envelope. We also demonstrate how the general formulation and algorithm for a reactive system can be simplified to a non-reactive one. We finally test the proposed formulations and algorithms with four distinctly different examples. The first example is bubble point calculation of CO_2-NaCl brine at constant T using the $\gamma-\phi$ approach, leading to vapor-liquid equilibrium (VLE) Pxy diagrams at several temperatures. The second is the calculation of solid solubility limit and construction of a Txy solid-liquid equilibrium (SLE) diagram using a γ model. The third is the construction of complete PT phase envelopes for a system with the alkene reaction. The last is the PT phase envelope of a hydrocarbon mixture using the saturation RAND reduced to non-reactive systems.

It is worthwhile to note that methodologies for saturation point calculation and phase diagram construction involving chemical reactions are rather scattered around the different scientific domains, and they are usually tailored to specific applications. SLE involving brine and solid salts, for instance, is usually solved through the law of mass action [17], whereas, in chemical engineering, there are distinct methodologies for VLE [18, 19] and SLE [20]. Hence, we comment on existing algorithms to solve problems similar to the selected examples in Section 3 (Results and Discussion).

2. Methodology

2.1. Definition of the Saturation Point Problem in Reactive Systems

In the following derivations, we focus on the development of algorithms for two-phase saturation problems. In non-reactive systems, these problems usually consist of $N_C + 2$ working variables, i.e., mole fractions of phase j ($\boldsymbol{x}_j$) [21] or K-factors [22, 23], T, and P. They are determined by $N_C + 2$ working equations, usually N_C chemical potential equalities, a summation equation, and a specification equation, provided that the phase amount of one of the phases (β_j^{spec}) and the feed composition ($\boldsymbol{z}$) are specified. Reactive systems in turn have the peculiarity that mole numbers of the N_C components ($\boldsymbol{n}$) are not conserved. Rather, in the non-stoichiometric paradigm [1] element amounts ($\boldsymbol{b}$) of the N_E elements are the fixed quantities. As a result, dimensional phase amounts, defined as $\beta_j = \sum_{i=1}^{N_C} n_{i,j}$, are no longer conserved, since the advancement of a reaction in a given phase might change β, hence the need for more convenient variables and specifications to treat reactive problems. The derivations presented in the course of the next sections rely on new variables and concepts, which we introduce here.

First, it is convenient to define the element amount of phase j (α_j) and the element fraction vector of phase j ($\boldsymbol{e}_j$) for all N_P phases. They are related to the original β_j and $\boldsymbol{x}_j$ by the following relations

$$\alpha_j = \beta_j \sum_{k=1}^{N_E} \sum_{i=1}^{N_C} \mathcal{A}_{k,i} x_{i,j} \tag{1a}$$

$$e_{k,j} = \sum_{i=1}^{N_C} \mathcal{A}_{k,i} x_{i,j} \tag{1b}$$

where $\mathcal{A}$ is the formula matrix. As a consequence of the definition of α_j, we have that

$$\sum_{j=1}^{N_P} \alpha_j = \sum_{k=1}^{N_E} b_k \tag{2}$$

and this relationship is analogous to that of β_j and $\boldsymbol{z}$ in the non-reactive case, i.e., $\sum_{j=1}^{N_P} \beta_j = \sum_{i=1}^{N_C} z_i$.

It is also important to note that $\boldsymbol{e}_j$ cannot be strictly interpreted as an element fraction, as it is not normalized. Nevertheless, the definition of $\boldsymbol{e}_j$ facilitates the development of the algorithm, especially in Section 2.3. We define the K-factors of elements ($\boldsymbol{K}^e$) in an analogous manner to the conventional component-based K-factors:

$$K_k^e = \frac{e_{k,1}}{e_{k,2}} \tag{3}$$

In the above equation, subscript 1 refers to the incipient phase and subscript 2 refers to the bulk phase. Although $\boldsymbol{e}_j$ used in the $\boldsymbol{K}^e$ definition is proportional, but not equal to the elemental mole fraction, $\boldsymbol{K}^e$ retains one important feature of the conventional K-factors, i.e., being equal to 1 at the critical point.

Finally, even though the dimensional β_j is not conserved during the calculation, , the relative value of phase amounts ($\beta_j^r = \beta_j / \sum_{j=1}^{N_P} \beta_j$) is still valid as a specification, since it can be kept constant. Hence, the intensive state of the reactive problem can be analyzed under two different paradigms, namely the element-based phase fraction ($\alpha_j^r = \alpha_j / \sum_{j=1}^{N_P} \alpha_j$) or the component-based fraction of a phase (β_j^r), whereas only α_j is meaningful in the determination of the extensive state of reactive systems.

Overall, the analysis of degrees of freedom of the two-phase saturation problem in reactive systems shows that two extra working variables appear in comparison to the non-reactive one: the changing β_j of the two phases. This leads to a total of $N_C + 4$ working variables. Hence, two extra equations are needed to close the problem in comparison to the non-reactive one.

2.2. Derivation of the Saturation RAND

The RAND method was originally developed to solve phase equilibrium problems by the minimization of G at constant T, P and mole numbers of the N_E elements present in the system ($\boldsymbol{b}$). The method is obtained by transforming the Gibbs energy minimization problem into a Lagrangian problem with the addition

of an element conservation constraint:

$$\mathcal{L}(\boldsymbol{n}, \lambda) = \sum_{j=1}^{N_P} \boldsymbol{n}_j^{\mathrm{T}} \boldsymbol{\mu}_j - \hat{\lambda}^{\mathrm{T}} \left(\mathcal{A} \sum_{j=1}^{N_P} \boldsymbol{n}_j - \boldsymbol{b} \right) \quad (4)$$

In the equation above, $\boldsymbol{n}_j$ is the vector for the mole number of all N_C components in a given phase j, $\boldsymbol{\mu}_j$ is the chemical potential vector of all N_C components in a given phase j, $\hat{\lambda}$ is the vector of dimensional Lagrange multipliers related to all N_E element conservation constraints, and $\mathcal{A}$ is the formula matrix. In the original RAND derivation, the stationary conditions of the problem are obtained for $\boldsymbol{n}$ and $\hat{\lambda}$. The stationary conditions in the saturation algorithm can be obtained for the working variables $\boldsymbol{x}_j$, i.e., the mole fraction of all N_C components in phase j. We then have the following stationary conditions (knowing that $n_{i,j} = \beta_j x_{i,j}$):

$$\frac{\partial \mathcal{L}}{\partial x_{i,j}} = \mu_{i,j} - \sum_{k=1}^{N_E} \mathcal{A}_{k,i} \hat{\lambda}_k = 0,$$
$$i \in [1, \cdots, N_C], \ j \in [1, \cdots, N_P] \quad (5\text{a})$$

$$\frac{\partial \mathcal{L}}{\partial \lambda_k} = - \sum_{i=1}^{N_C} \mathcal{A}_{i,k} \sum_{j=1}^{N_P} \beta_j x_{i,j} + b_k = 0, \ k \in [1, \cdots, N_E] \quad (5\text{b})$$

Similar to the general RAND procedure, we can linearize Equation 5a with respect to the working variables $\boldsymbol{x}_j$ in addition to T, P and λ (dimensionless Lagrange multiplier):

$$\frac{\boldsymbol{\mu}_j}{RT} + \frac{1}{RT} \frac{\partial \boldsymbol{\mu}_j}{\partial \boldsymbol{x}_j} \Delta \boldsymbol{x}_j + \frac{\partial \boldsymbol{\mu}_j}{\partial T} \Delta T + \frac{\partial \boldsymbol{\mu}_j}{\partial P} \Delta P - \mathcal{A}^{\mathrm{T}} \lambda - \mathcal{A}^{\mathrm{T}} \Delta \lambda = \boldsymbol{0} \quad (6)$$

This equation is inverted to isolate $\Delta \boldsymbol{x}_j$ with the aid of the $\boldsymbol{M}$ matrix for a phase j, as in previous derivations of the modified RAND method [12, 24]. This is possible because the derivatives of chemical potential w.r.t. x are equivalent to those w.r.t. n, if variables in vector $\boldsymbol{x}_j$ are considered independent (See Supplementary Material). $\boldsymbol{M}_j$ is defined as follows:

$$\boldsymbol{M}_j = \boldsymbol{m}_j^{-1} \quad (7)$$

The terms of the $\boldsymbol{m}_j$ are in turn

$$m_{p,q,j} = \beta_j \left(\frac{1}{RT} \frac{\partial \mu_{p,j}}{\partial n_{q,j}} + 1 \right) \quad (8)$$

Then, we have

$$\Delta \boldsymbol{x}_j = \boldsymbol{M}_j \left(\mathcal{A}^{\mathrm{T}} \lambda - \frac{\boldsymbol{\mu}_j}{RT} + \mathcal{A}^{\mathrm{T}} \Delta \lambda - \boldsymbol{\tau}_j \Delta T - \boldsymbol{\nu}_j \Delta P \right) \quad (9)$$

with $\boldsymbol{\tau}_j = \frac{\partial \boldsymbol{\mu}_j}{\partial T}$ and $\boldsymbol{\nu}_j = \frac{\partial \boldsymbol{\mu}_j}{\partial P}$. From the definition of the $\boldsymbol{M}$ matrix, we know that $\boldsymbol{1}^{\mathrm{T}} \boldsymbol{M}_j = \boldsymbol{x}_j^{\mathrm{T}}$. Furthermore, the mole fractions should always add up to one and, as a consequence, $\boldsymbol{1}^{\mathrm{T}} \Delta \boldsymbol{x}_j = 0$. Hence, the multiplication of Equation 9 from $\boldsymbol{1}^{\mathrm{T}}$ from the left

side leads to the following equation for every phase j:

$$\boldsymbol{x}_j^{\mathrm{T}} \left(\mathcal{A}^{\mathrm{T}} \Delta \lambda - \boldsymbol{\tau}_j \Delta T - \boldsymbol{\nu}_j \Delta P \right) = \sum_{i=1}^{N_C} x_{i,j} \left(\frac{\mu_{i,j}}{RT} - \sum_{k=1}^{N_E} \mathcal{A}_{k,i} \lambda_k \right) \quad (10)$$

Another set of equations is obtained from manipulation of Equation 5b. First, we linearize it with respect to $\boldsymbol{x}_j$ and β_j, the working variables of the problem:

$$-\mathcal{A} \sum_{j=1}^{N_P} \left(\beta_j \boldsymbol{x}_j + \beta_j \Delta \boldsymbol{x}_j + \boldsymbol{x}_j \Delta \beta_j \right) + \boldsymbol{b} = \boldsymbol{0} \quad (11)$$

Provided that the initial values of $x_{i,j}$ and β_j meet the element balance and that the system is closed, it follows that

$$\mathcal{A} \sum_{j=1}^{N_P} \left(\beta_j \Delta \boldsymbol{x}_j + \boldsymbol{x}_j \Delta \beta_j \right) = \boldsymbol{0} \quad (12)$$

Substitution of the expression of $\Delta \boldsymbol{x}_j$ from Equation 9 into Equation 12 leads to a set of mass balance equations similar to the original RAND method, since $\Delta \boldsymbol{n}_j = \beta_j \Delta \boldsymbol{x}_j + \boldsymbol{x}_j \Delta \beta_j$. They are:

$$\mathcal{A} \left(\sum_{j=1}^{N_P} \beta_j \boldsymbol{M}_j \right) \mathcal{A}^{\mathrm{T}} \Delta \lambda + \mathcal{A} \boldsymbol{x}_1 \Delta \beta_1 + \mathcal{A} \boldsymbol{x}_2 \Delta \beta_2 -$$
$$\mathcal{A} \left(\sum_{j=1}^{N_P} \beta_j \boldsymbol{M}_j \boldsymbol{\tau}_j \right) \Delta T - \mathcal{A} \left(\sum_{j=1}^{N_P} \beta_j \boldsymbol{M}_j \boldsymbol{\nu}_j \right) \Delta P =$$
$$\mathcal{A} \sum_{j=1}^{N_P} \beta_j \boldsymbol{M}_j \left(\frac{\boldsymbol{\mu}_j}{RT} - \mathcal{A}^{\mathrm{T}} \lambda \right) \quad (13)$$

However, two specification equations are still needed. One specification equation is related to the phase fractions, such as specification for α_j or β_j^r. We choose to use the generic variable X_s^m for the variable (α_j or β_j^r) to be specified and S^m for the value of the specification:

$$-\left(\frac{\partial X_s^m}{\partial \lambda} \right)^{\mathrm{T}} \Delta \lambda - \frac{\partial X_s^m}{\partial \beta_1} \Delta \beta_1 - \frac{\partial X_s^m}{\partial \beta_2} \Delta \beta_2 - \frac{\partial X_s^m}{\partial T} \Delta T$$
$$- \frac{\partial X_s^m}{\partial P} \Delta P = X_s^m - S^m \quad (14)$$

The other specification equation is related to the working variables T, P, and λ, or a set of variables depending on them, such as $\ln K_k^e$. We use the generic variable X_s^t to denote one of these variables and the corresponding specified value S^t

$$-\left(\frac{\partial X_s^t}{\partial \lambda} \right)^{\mathrm{T}} \Delta \lambda - \frac{\partial X_s^t}{\partial \beta_1} \Delta \beta_1 - \frac{\partial X_s^t}{\partial \beta_2} \Delta \beta_2 - \frac{\partial X_s^t}{\partial T} \Delta T$$
$$- \frac{\partial X_s^t}{\partial P} \Delta P = X_s^t - S^t \quad (15)$$

Combining the specification equations with Equation 10 for each phase and Equation 13, we arrive at the following system

of equations:

$$
\begin{bmatrix}
\mathcal{A}M^s\mathcal{A}^T & \mathcal{A}x_1 & \mathcal{A}x_2 & -\mathcal{A}\tau^s & -\mathcal{A}v^s \\
(\mathcal{A}x_1)^T & 0 & 0 & -x_1^T\tau_1 & -x_1^T v_1 \\
(\mathcal{A}x_2)^T & 0 & 0 & -x_2^T\tau_2 & -x_2^T v_2 \\
-\left(\frac{\partial X_s^m}{\partial\lambda}\right)^T & -\frac{\partial X_s^m}{\partial\beta_1} & -\frac{\partial X_s^m}{\partial\beta_2} & -\frac{\partial X_s^m}{\partial T} & -\frac{\partial X_s^m}{\partial P} \\
-\left(\frac{\partial X_s^t}{\partial\lambda}\right)^T & -\frac{\partial X_s^t}{\partial\beta_1} & -\frac{\partial X_s^t}{\partial\beta_2} & -\frac{\partial X_s^t}{\partial T} & -\frac{\partial X_s^t}{\partial P}
\end{bmatrix}
\begin{bmatrix}
\Delta\lambda \\
\Delta\beta_1 \\
\Delta\beta_2 \\
\Delta T \\
\Delta P
\end{bmatrix}
= R \quad (16)
$$

where

$$
M^s = \sum_{j=1}^{N_P} \beta_j M_j \tag{17a}
$$

$$
\tau^s = \sum_{j=1}^{N_P} \beta_j M_j \tau_j \tag{17b}
$$

$$
v^s = \sum_{j=1}^{N_P} \beta_j M_j v_j \tag{17c}
$$

and the residual vector is

$$
R = \begin{bmatrix}
\mathcal{A}\sum_{j=1}^{N_P}\beta_j M_j\left(\frac{\mu_j}{RT} - \mathcal{A}^T\lambda\right) \\
\sum_{i=1}^{N_C} x_{i,1}\left(\frac{\mu_{i,1}}{RT} - \sum_{k=1}^{N_E}\mathcal{A}_{k,i}\lambda_k\right) \\
\sum_{i=1}^{N_C} x_{i,2}\left(\frac{\mu_{i,2}}{RT} - \sum_{k=1}^{N_E}\mathcal{A}_{k,i}\lambda_k\right) \\
X_s^m - S^m \\
X_s^t - S^t
\end{bmatrix} \tag{18}
$$

After solution of Equation 16 the change in mole numbers of a phase j can be obtained by

$$
\Delta n_j = x_j\Delta\beta_j + \beta_j M_j\left(\mathcal{A}^T\lambda - \frac{\mu_j}{RT} + \mathcal{A}^T\Delta\lambda - \tau_j\Delta T - v_j\Delta P\right) \tag{19}
$$

with x_j being updated afterwards by $x_j = n_j/\beta_j$. For incipient phases ($\beta_j = 0$ or $\alpha_j = 0$), Equation 19 reduces to Equation 9, and the mole fractions can be directly updated from it.

Some comments need to be made with regards to Equation 16. First, the derivation is performed so that the final system of equations is written in terms of updates of all working variables, and this is different from the usual derivation of the RAND method, which has a final system of equations including λ, instead of $\Delta\lambda$. Derivations with $\Delta\lambda$ are also available in the literature [11] and the reason behind the choice here is the convenience it brings when calculating the sensitivity vector (further discussed in Section 2.3.2). Second, any variable of the problem can be specified in the two specification equations of Equation 16. If the specified variable is already present in the final system of equations (i.e., it belongs to the set $v = [\lambda, \beta_1, \beta_2, T, P]$), the derivative vector ($\frac{\partial X_s}{\partial v}$) should be a vector of zeros with the value of 1 in the row related to the selected variable. If X_s is not a working variable of Equation 16, i.e., $X_s \notin v$, nor is a direct function of any of the variables in v, such as $X_s = \ln K_k^e$ or $X_s = \alpha_j$, a chain rule w.r.t. mole fractions of the components (x_j) is needed, such that

$$
\Delta X_s = \sum_{i=1}^{N_C}\sum_{j=1}^{N_P} \frac{\partial X_s}{\partial x_{i,j}}\Delta x_{i,j} \tag{20}
$$

The equation can be fully incorporated to the system solving step, if followed by substitution of Equation 9, which describes how a change in $x_{i,j}$ is represented in terms of the variable space from set v. Analogous procedures are needed in the derivation steps of working equations in RAND (such as substitution of Equation 9 into Equation 12). The underlying principle of the method is the recasting of the phase equilibrium equations (f), originally written in terms of x_j or n_j, i.e., $f = f(x_j)$, in a new form $g = g(\lambda, \beta)$, by acknowledging that $x_j = x_j(\lambda, \beta)$.

In this work, we devised two types phase fraction specification: one for α_j and another one for β_j^r, being β_j^r the normalized value of β_j, such that $\beta_j^r = \beta_j/(\sum_{j=1}^{N_P}\beta_j)$. The equation for α specification of phase 1 (α_1) is presented below (detailed derivation in the supplementary material):

$$
\mathbf{1}^T\mathcal{A}x_1\Delta\beta_1 + \beta_1\mathbf{1}^T\mathcal{A}M_1\mathcal{A}^T\Delta\lambda - \beta_1\mathbf{1}^T\mathcal{A}M_1\tau_1\Delta T
$$
$$
- \beta_1\mathbf{1}^T\mathcal{A}M_1 v_1\Delta P = \beta_1\mathbf{1}^T\mathcal{A}M_1\left(\frac{\mu_1}{RT} - \mathcal{A}^T\lambda\right) \quad (21)
$$

It is interesting to note that if α_1 is specified to be zero, the above equation becomes $\Delta\beta_1 = 0$, and this is the only case in which there is a direct equivalence between α and β. The alternative equation for β^r specification of phase 1 is:

$$
\left(\beta_1^{r,\text{spec}} - 1\right)\Delta\beta_1 + \beta_1^{r,\text{spec}}\Delta\beta_2 = 0 \tag{22}
$$

As it only involves variables that are present in v, no chain rule w.r.t. x_j is needed. For the other specification equation, we have chosen T, P and $\ln K_k^e$ as possible specified variables. It should be noted that λ can also be used as specified variables. The equations for T and P are trivial, since they belong to set v. The equation for $\ln K_k^e$ requires some derivation, and it is discussed in Section 2.3.1.

The iterative procedure of the saturation RAND, from initial estimates in T, P, x_j, β_1, β_2 and λ, is:

1. Calculate M_j, τ_j, v_j and μ_j for the two phases;
2. Solve Equation 16 for $\Delta\lambda$, $\Delta\beta_1$, $\Delta\beta_2$, ΔT, and ΔP;
3. Calculate the update in n_j from Equation 19 (for incipient phases, calculate Δx_j through Equation 9);
4. Update the values of T, P, β_1, β_2, λ and n_j (occasionally reducing the step to avoid negative values of T, P, β_1, β_2, or n_j);
5. Calculate mole fractions by $x_j = n_j/\beta_j$;
6. Check convergence. If achieved, stop. If not achieved, go back to step 1.

2.3. Phase Envelope Construction

The algorithm presented in the previous section is already suitable for calculation of individual points in curves at constant element phase amount of one of the phases (α_j) or component phase fraction (β_j^r). Therefore, tasks such as calculating the solubility of a certain component through a range of T or P in a bulk phase can be successfully performed by coupling the saturation RAND with a grid in T, P or in the global composition of an element. The results presented in Sections 3.1 and 3.2 were obtained following such procedures.

However, it is often desirable to have a robust algorithm that can construct the PT phase envelope at different phase fractions automatically. The classical example of such an algorithm for non-reactive systems is that of Michelsen [22, 23]. In his algorithm, one variable among the set $X = [\ln T, \ln P, \ln K]$ is selected as the specification variable X_S of the core saturation algorithm based on the sensitivity of each variable in X w.r.t. S. First, an initial phase equilibrium calculation at constant β is performed at whichever X_S (usually P at low values). Then, a vector of sensitivities $\partial X/\partial S$ is calculated, and the most sensitive variable (the one that has the maximum absolute value of $\partial X/\partial S$) is selected as specification. The algorithm moves to the next point in the phase envelope by an increment in S, using initial estimates generated by

$$X_{l+1} = X_l + \frac{\partial X_l}{\partial S} \Delta S \qquad (23)$$

Here, subscript l and $l+1$ denote the current and the next points, respectively. By doing so, Michelsen devised a simple yet efficient strategy for plotting phase envelopes and quality lines of non-reactive two-phase mixtures at constant z.

In this section, we describe how to extend the standalone saturation RAND formulation, derived in Section 2.2, to PT phase envelope construction using Michelsen's methodology [22, 23]. Results from the RAND-based phase envelope algorithms are presented in Section 3.3 and Section 3.4.

2.3.1. K-factor Specification

Michelsen [21] recommended to use $\ln K$ as working variables in his phase envelope algorithm using Newton's method although he shows that a formulation using mole fractions as working variables is also possible. He further pointed out that $\ln K$ can be specified, just as the more common specifications for T and P, in the phase envelope construction.

One of the main nuisances in phase envelope calculation is the risk of converging to the trivial solution ($x_{i,1} = x_{i,2}$, and $\ln K_i = 0, \forall i$). Working with specified $\ln K_i$ of a certain component prevents this scenario, since the trivial solution does not satisfy the set of equations, if we set $\ln K_i^{\text{spec}} \neq 0$. This is particularly useful close to the critical point and a phase envelope algorithm working with specified $\ln K$ is therefore more robust.

For a reactive system, we use the K-factors for the elements (K_k^e), as introduced in Section 2.1, in place of $\ln K$:

$$\ln K_k^e = \ln e_{k,1} - \ln e_{k,2} \qquad (24)$$

Then, a specification equation ($\ln K_k^e - S = 0$) can be added used as the working variable specification equation (Equation 15). To incorporate this specification to the problem, however, we have to express $\ln K_k^e$ in terms of vector v in the RAND formulation, by the transformation described in Equation 20. From the definition of $\ln K_k^e$, it follows that

$$\Delta \ln K_k^e = \frac{1}{e_{k,1}} \Delta e_{k,1} - \frac{1}{e_{k,2}} \Delta e_{k,2} \qquad (25)$$

which can be written in terms of $x_{i,j}$ with the aid of the defini-

tion of element fractions (Equation 1b)

$$\Delta \ln K_k^e = \frac{1}{e_{k,1}} \mathscr{A}_k \Delta x_1 - \frac{1}{e_{k,2}} \mathscr{A}_k \Delta x_2 \qquad (26)$$

Comparing Equation 26 and Equation 20, we see that:

$$\left(\frac{\partial \ln K_k^e}{\partial x_1} \right)^{\text{T}} = \frac{1}{e_{k,1}} \mathscr{A}_k; \quad \left(\frac{\partial \ln K_k^e}{\partial x_2} \right)^{\text{T}} = -\frac{1}{e_{k,2}} \mathscr{A}_k \qquad (27)$$

with $\mathscr{A}_k$ being the row of length N_C of the formula matrix corresponding to element k. Other partial derivatives w.r.t. to the working variables (vector v) of the equation solving step of the saturation RAND (Equation 16) are obtained by substitution of Equation 9 into Equation 26 for every element k. They are collected in the following matrix:

$$\frac{\partial \ln K^e}{\partial v} = \begin{bmatrix} B_{\lambda,1}^e - B_{\lambda,2}^e & 0 & 0 & B_{T,1}^e - B_{T,2}^e & B_{P,1}^e - B_{P,2}^e \end{bmatrix} \qquad (28)$$

Matrix B_j^e, in turn, is a matrix collecting the derivatives of $\ln e_j$ w.r.t. to the working variables from v for certain phase j, with the exception of β_1 and β_2, for which the derivative of $\ln K_k^e$ is zero:

$$B_j^e = \begin{bmatrix} B_{\lambda,j}^e & B_{T,j}^e & B_{P,j}^e \end{bmatrix} \qquad (29a)$$

$$B_j^e = [\text{diag}(1/e_j)\mathscr{A}M_j\mathscr{A}^{\text{T}}, \ -(1/e_j)\mathscr{A}M_j\tau_j,$$
$$- (1/e_j)\mathscr{A}M_j v_j] \qquad (29b)$$

In the above equation, $\text{diag}(1/e_j)$ represents the diagonal matrix of vector $(1/e_j)$, containing the inverse element fractions of each phase. Hence, the specification equation (Equation 15) for a given $\ln K_k^e$ becomes

$$- \frac{\partial \ln K_k^e}{\partial \lambda} \Delta \lambda - \frac{\partial \ln K_k^e}{\partial T} \Delta T - \frac{\partial \ln K_k^e}{\partial P} \Delta P = \ln K_k^e - S$$
$$+ \text{diag}(1/e_1)\mathscr{A}M_1 \left(\mathscr{A}^{\text{T}}\lambda - \frac{\mu_1}{RT} \right) - \text{diag}(1/e_2)\mathscr{A}M_2 \left(\mathscr{A}^{\text{T}}\lambda - \frac{\mu_2}{RT} \right) \qquad (30)$$

2.3.2. Sensitivity Vector of the Working Variables

The remaining step needed to employ Michelsen's phase envelope strategy [22, 23] is to calculate the sensitivity of the variables. A sensitivity vector with respect to $\lambda, \beta_1, \beta_2, \ln T$ and $\ln P$ (denoted by X^{RAND}) can be obtained directly from the following system of equations:

$$\frac{\partial R}{\partial X^{\text{RAND}}} \frac{\partial X^{\text{RAND}}}{\partial S} = -\frac{\partial R}{\partial S} \qquad (31)$$

In the above equation, $\partial R/X^{\text{RAND}}$ is the matrix from the left-hand side of Equation 16 at the solution of the saturation problem, with τ_j and v_j substituted by $T \times \tau_j$ and $P \times v_j$, respectively, and $\partial R/S$ is a vector of zeros with 1 at the last row (N_E+N_P+2).

The components of $\partial X^{\text{RAND}}/\partial S$ are:

$$\frac{\partial X_l^{\text{RAND}}}{\partial S} = \begin{cases} \frac{\partial \lambda}{\partial S}, & l \in [1, \cdots, N_E] \\ \frac{\partial \beta_1}{\partial S}, & l = N_E + 1 \\ \frac{\partial \beta_2}{\partial S}, & l = N_E + 2 \\ \frac{\partial \ln T}{\partial S}, & l = N_E + 3 \\ \frac{\partial \ln P}{\partial S}, & l = N_E + 4 \end{cases} \quad (32)$$

The components of the sensitivity vector used in the phase envelope calculation ($\partial X/\partial S$) can be obtained from $\partial X^{\text{RAND}}/\partial S$ as:

$$\frac{\partial X_l}{\partial S} = \begin{cases} \frac{\partial \ln K_l^e}{\partial \lambda}\frac{\partial \lambda}{\partial S} + \frac{\partial \ln K_l^e}{\partial \ln T}\frac{\partial \ln T}{\partial S} + \frac{\partial \ln K_l^e}{\partial \ln P}\frac{\partial \ln P}{\partial S}, & l \in [1, \cdots, N_E] \\ \frac{\partial \ln T}{\partial S}, & l = N_E + 1 \\ \frac{\partial \ln P}{\partial S}, & l = N_E + 2 \end{cases}$$

$$(33)$$

Derivatives of $\ln K^e$ w.r.t. $\ln T$, $\ln P$ and λ can be obtained from Equation 28, with the substitution of τ_j and ν_j by $T \times \tau_j$ and $P \times \nu_j$, respectively. The vector composed of the elements from the above equation can be readily used in the same way as the sensitivity vector proposed by Michelsen. After selecting the specification variable among $\ln K^e$, $\ln T$ and $\ln P$, the other ones can be updated either using $\partial X/\partial S$ or $\partial X^{\text{RAND}}/\partial S$, depending on the type of variable, as in Equation 23.

The selection of T, P and $\ln K^e$ as possible variables to be specified in the phase envelope construction is justified for the sake of consistency with Michelsen's phase envelope algorithm and for the advantages that the $\ln K^e$ specification brings to the problem. We emphasize here that it is also possible to specify λ, but it is advantageous to specify $\ln K^e$ around the critical point. In any case, the sensitivity of the solution w.r.t. λ is still calculated to generate initial estimates for this set of variables.

2.3.3. Calculation Procedure

The phase envelope calculation starts at a low pressure point where the solution is easy to find for the specified α or β^r. It should be possible to develop an optimal procedure for the solution at the low pressure as used for the non-reactive case [22, 23]. In this work, we simply used a flash-based approach to locate the solution. We distinguish two situations: for α or β^r equal to 0 or 1, we solve a single-phase chemical equilibrium problem at an initial estimate of T and the specified P, and initialize the incipient phase composition using the minimum point composition obtained in in the tangent plane analysis; for α or β^r between 0 and 1, we search T using two-phase CPE flash to meet the α or β^r specification.

The procedure after initialization is as follows:

1. Perform a saturation point calculation at one of the specified variables T, P or $\ln K^e$, using the algorithm from Section 2.2. It is also possible to perform calculations at specified λ;

2. Calculate the sensitivities of the possible specification variables (Equations 32 and 33);

3. Check the maximum absolute value of $\ln K^e$. If greater than a threshold close to zero, continue to step 4. If not, continue to step 6;

4. Check if T and P have satisfied their stopping criteria, stop. If not, go to step 5;

5. Select the most sensitive variable, increase by a step and calculate initial estimates for the RAND working variables (T, P and λ) using Equation 23. Go back to step 1;

6. Invert the phases by multiplying both the specified value of $\ln K^e$ and the set of $\ln K$ by -1. Calculate initial guesses for the mole fractions of the incipient phase (the one whose α is not specified) by $x_{i,1} = K_i x_{1,2}$. Calculate initial estimates for the RAND working variables (T, P and λ) by Equation 23. Go to step 1.

2.4. Simplification to Non-Reactive Systems

Paterson et al. [12] showed that the RAND algorithm can be simplified to solve non-reactive flash specification problems. Similarly, the saturation RAND can be applied to non-reactive cases, working as an alternative to saturation algorithms [22, 23] based on the Rachford-Rice equations [25]. In non-reactive systems, one species cannot be converted into another. Therefore, the smallest number of species that determines the state of the whole system is N_C, in contrast to N_E in the reactive case. The formula matrix $\mathcal{A}$ (originally of size $N_E \times N_C$ in the reactive case) corresponds the identity matrix I of size $N_C \times N_C$ in the non-reactive case. Another modification is that Equation 10 for both phases can be combined to generate a specification equation analogous to the Rachford-Rice summation equation (see Supplementary Material). Equation 16, after transformation, takes the form:

$$\begin{bmatrix} M_j^s & -\tau^s & -\nu^s \\ \sum_{j=1}^{N_P=2} x_j^T & -\sum_{j=1}^{N_P=2} x_j^T \tau_j & -\sum_{j=1}^{N_P=2} x_j^T \nu_j \\ -\left(\frac{\partial X_s}{\partial \lambda}\right)^T & -\frac{\partial X_s}{\partial T} & -\frac{\partial X_s}{\partial P} \end{bmatrix} \begin{bmatrix} \Delta\lambda \\ \Delta T \\ \Delta P \end{bmatrix} =$$
$$\begin{bmatrix} \sum_{j=1}^{N_P=2} \beta_j^{\text{spec}} M_j \left(\frac{\mu_j}{RT} - \lambda\right) \\ \sum_{j=1}^{N_P=2} \sum_{i=1}^{N_C} x_{i,j} \left(\frac{\mu_{i,j}}{RT} - \lambda_i\right) \\ X_s - S \end{bmatrix} \quad (34)$$

with Δx_j and Δn_j given by

$$\Delta x_j = M_j \left(\lambda - \frac{\mu_j}{RT} + \Delta\lambda - \tau_j \Delta T - \nu_j \Delta P\right) \quad (35a)$$

$$\Delta n_j = x_j \Delta\beta_j + \beta_j M_j \left(\lambda - \frac{\mu_j}{RT} + \Delta\lambda - \tau_j \Delta T - \nu_j \Delta P\right) \quad (35b)$$

Here, the symbols M^s, τ^s and ν^s have the same meaning as in Equations 17a, 17b and 17c, respectively. If the specified variable is one of the working variables of Equation 34 (i.e., it belongs to $\nu = [\lambda, T, P]$) the derivative vector $\frac{\partial X_s}{\partial \nu}$ is a vector of zeros with the value of 1 in the row related to the selected variable. The specification of $\ln K$ of a certain component i would lead to the following specification equation:

$$-\frac{\partial \ln K_i}{\partial \lambda}\Delta\lambda - \frac{\partial \ln K_i}{\partial T}\Delta T - \frac{\partial \ln K_i}{\partial P}\Delta P = \ln K_i - S$$
$$+ \text{diag}(1/x_1)M_1\left(\lambda - \frac{\mu_1}{RT}\right) - \text{diag}(1/x_2)M_2\left(\lambda - \frac{\mu_2}{RT}\right) \quad (36)$$

With $\mathrm{diag}\left(1/x_j\right)$ representing the diagonal matrix of vector $\left(1/x_j\right)$, containing the inverse mole fractions of phase j. The derivatives of $\ln K_i$ with respect to λ, T and P are:

$$\frac{\partial \ln \mathbf{K}}{\partial \mathbf{v}} = \begin{bmatrix} \mathbf{B}^c_{\lambda,1} - \mathbf{B}^c_{\lambda,2} & \mathbf{B}^c_{T,1} - \mathbf{B}^c_{T,2} & \mathbf{B}^c_{P,1} - \mathbf{B}^c_{P,2} \end{bmatrix} \quad (37)$$

with

$$\mathbf{B}^c_j = \begin{bmatrix} \mathbf{B}^c_{\lambda,j} & \mathbf{B}^c_{T,j} & \mathbf{B}^c_{P,j} \end{bmatrix} \quad (38a)$$

$$\mathbf{B}^c_j = \begin{bmatrix} \mathrm{diag}(1/x_j)\mathbf{M}_j & -(1/x_j)\mathbf{M}_j\boldsymbol{\tau}_j & -(1/x_j)\mathbf{M}_j\boldsymbol{\nu}_j \end{bmatrix} \quad (38b)$$

The sensitivity vector can be calculated with a procedure analogous to the one described in the previous section, with two sensitivity vectors, one for the inner RAND loop and another one relating $\ln \mathbf{K}$, $\ln T$ and $\ln P$.
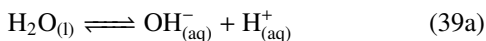
3. Results and Discussion

3.1. Pxy Phase Diagram: CO₂ Solubility in Brine

The correct prediction of CO_2 solubility in brines is central to reliable simulations of CO_2 injection in natural geological formations, such as saline aquifers and depleted oil reservoirs [26]. This task is made complex by the number of speciation reactions that can occur in the aqueous phase. Therefore, modeling research on the interaction between the injected CO_2 and natural environments resort to CPE calculations, focusing on the effect the reactions play in the phase behavior [27]. However, the modeling work involving chemical reactions in this area usually treats the problem under the flash paradigm.

The most notable examples of systematic CPE algorithms for saturation points in VLE are the works of Doherty et al. during the 1980s and 1990s. In 1988, Barbosa and Doherty [28] presented a set of new composition variables accounting for the reduced number of degrees of freedom in CPE due to reactions in order to improve the representation of reactive phase diagrams. In the paper, they explain the underlying thermodynamic theory of the variable transformation and outline an algorithm used to generate reactive Txy phase diagrams, which was based on solving the law of mass action and equalities of fugacities. Their method was only applied to incipient conditions. This research line was then continued by the works of Ung and Doherty, who derived a new variable transformation and new algorithms for Txy phase diagrams [19]. The authors also provided expressions for thermodynamic state functions that accounted for chemical reactions [18]. There are examples of later works that followed their approach [29, 30, 31]. In addition to those authors, Perez-Cisneros et al. [32] have also worked on the topic, but within the non-stoichiometric framework.

In this example, we studied the CO_2 solubility in sodium chloride brines. The thermodynamic modeling followed a $\gamma - \phi$ approach with the Pitzer model [33, 34] for the aqueous phase and the Peng-Robinson [35] equation of state (EoS) for the CO_2-rich phase. The following three speciation reactions were considered:

$$\mathrm{H_2O_{(l)}} \rightleftharpoons \mathrm{OH^-_{(aq)}} + \mathrm{H^+_{(aq)}} \quad (39a)$$

$$\mathrm{CO^{2-}_{3,(aq)}} + \mathrm{H^+_{(aq)}} \rightleftharpoons \mathrm{HCO^-_{3,(aq)}} \quad (39b)$$

$$\mathrm{CO^{2-}_{3,(aq)}} + 2\,\mathrm{H^+_{(aq)}} \rightleftharpoons \mathrm{CO_{2,(aq)}} + \mathrm{H_2O_{(l)}} \quad (39c)$$
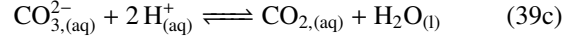
The reaction constant parameters were taken from the Pitzer database from PHREEQC [36]. Details on the thermodynamic modeling and parameters used can be found in the supplementary material to this paper. Overall, 8 species were present in the calculations (H_2O, OH^-, H^+, CO_2, HCO_3^-, CO_3^{-2}, Na^+, Cl^-). Combing this piece information with the amount of reactions, one arrives at 5 elements. Here, elements were selected as species present in the system, and they were CO_2, H^+, OH^-, Na^+ and Cl^-. The calculations here involve two phases, namely, a water-rich electrolyte-continaing phase, and a CO_2-rich fluid phase containing only H_2O and CO_2.

The element molar fraction of the CO_2-rich phase was fixed at 0 (i.e., $\alpha_g = \alpha^r_g = 0$), which coincides with $\beta_g = \beta^r_g = 0$, and the saturation pressure was calculated for a given composition of the bulk aqueous phase ($\alpha^r_{aq} = 1$ and $\alpha_{aq} = \sum_{k=1}^{N_E} b_k$) at a fixed T. Even though β_{aq} was not fixed, its change is negligible, since the speciation reactions involved species that were present in small amounts when compared to water and ultimately $\alpha_{aq} \approx \beta_{aq}$. The whole range of solubility was spanned by increasing the element amount of CO_2 in the bulk phase from one point to the other. The initial point had the following element specification: $b_{H^+} = 55.51$ mol, $b_{OH^-} = 55.51$ mol, $b_{CO_2} = 0$ mol, and b_{Na^+} and b_{Cl^-} corresponding to the specified NaCl molalities.

The results are displayed in Figure 1. Figures 1 (a), (b) and (c) show the molality of CO_2 in three different aqueous solutions (0 molal, 1 molal and 5 molal of NaCl) at the incipient condition of a CO_2 rich-phase at the temperature values of 323.2 K, 373.2 K and 413.2 K, respectively. Figures 1 (d), (e) and (f) show the molar fraction of water in the CO_2-rich phase in equilibrium with the brines shown in Figure 1 (a), (b) and (c), respectively. The type of phase diagram generated here falls into the category of a Pxy phase diagram, even though the compositions of the vapor and liquid phases are split in different series of plots.

The algorithm converges through a wide range of saturation pressures and is capable of capturing correctly the features of both phases of the system. The calculated results also agree with the experimental data in general. The largest deviations are found at higher temperatures (373.2 K and 413.2 K) and higher molalities (5 molal). Furthermore, the algorithm presents quadratic convergence close to the solution as illustrated by Figure 2. Figure 2 shows the maximum absolute value of the update among any of the variables x_j, β, T, P and λ through the iterations, here represented by the generic symbol $\Delta\xi$. The calculated points in Figure 2 correspond to all three NaCl molalities studied (0, 1 and 5 molal) at 413.2 K at the fixed CO_2 element amount of 0.19, and it is representative of the convergence behavior in other conditions as well. At the beginning of the calculation, the updates stay at a very high plateau until they reach second order convergence close to the solution. It is noteworthy that the pressure and composition derivatives of the Pitzer model were obtained by numerical differentiation.
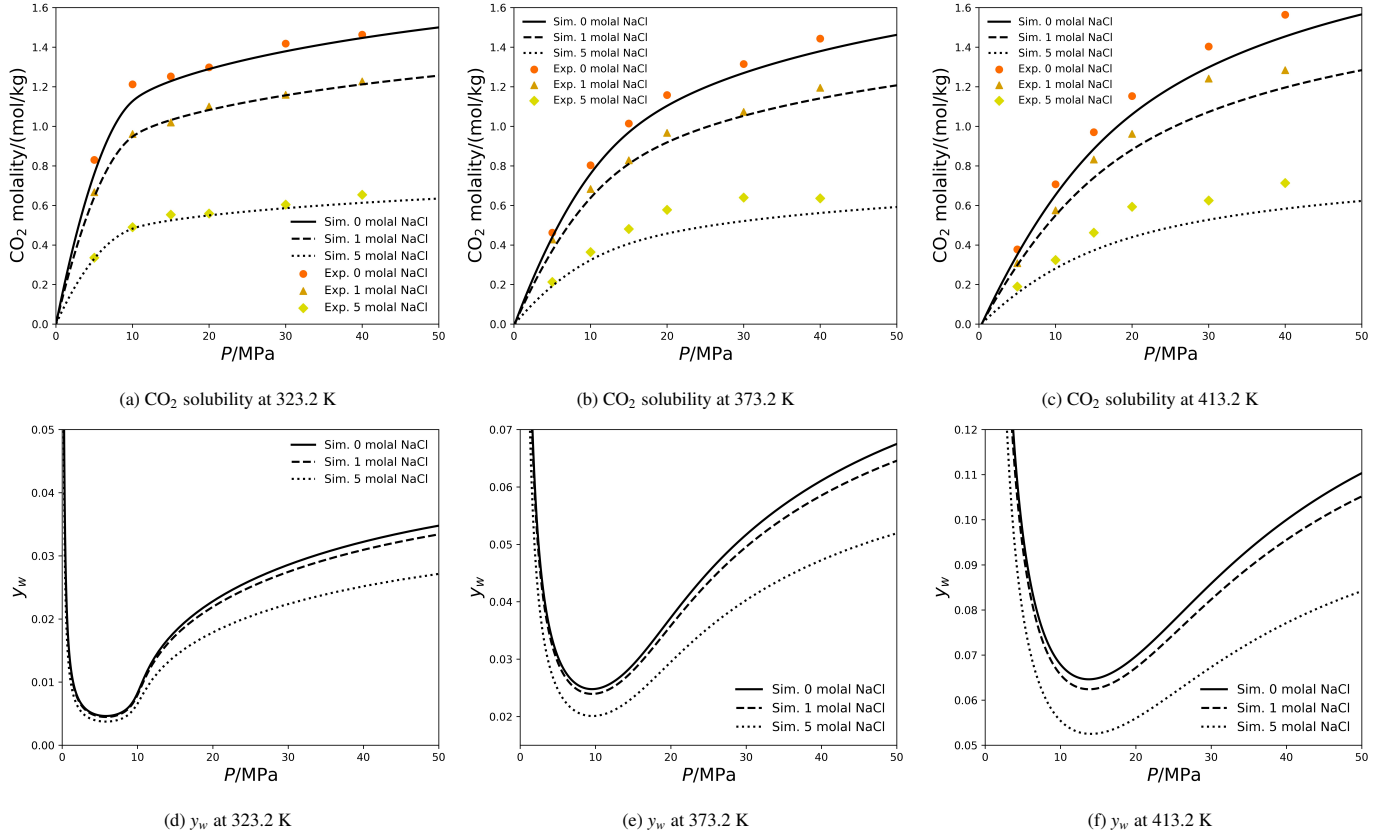
(a) CO_2 solubility at 323.2 K

(b) CO_2 solubility at 373.2 K

(c) CO_2 solubility at 413.2 K

(d) y_w at 323.2 K

(e) y_w at 373.2 K

(f) y_w at 413.2 K

Figure 1: CO_2 solubility in brine (Figures (a), (b) and (c) and mole fraction of water in the CO_2-rich fluid phase (Figures (d), (e) and (f)) at 323.2 K, 373.2 K and 413.2 K. Experimental data from Yan et al. [26].

Figure 2: Convergence behavior of the algorithm at 413.2 K and 0.19 element amount of CO_2 for the three molalities of NaCl studied (0, 1 and 5 molal).

3.2. Txy Phase Diagram: Solubility of Binary Salts

It is not rare that reactive mixtures undergo reactions that produce less soluble species that eventually precipitate. This phenomenon is behind mineral scaling [37], and it is also the driving force of reactive crystallization processes [7, 38]. In this type of problem, one is usually interested in calculating the value of given thermodynamic property (usually either temperature or concentration) that allows for the precipitation of a solid phase from a liquid solution. Here, the literature diverges in the saturation point methodology used, depending on the application. In electrolyte systems, in which speciation reactions take place in the aqueous phase, the main approach to solve this problem is the numerical solution of the law of mass action [17, 39]. Slaughter and Doherty's methdology [20], on the other hand, is mostly found in works discussing process engineering for the construction of SLE phase diagrams of molecular solids [7, 40, 41, 42]. Other noteworthy applications of SLE phase equilibrium algorithms are in materials science for the prediction of metal alloy phase behavior, the so-called Calphad approach [2].

In this example, we calculated the solubility of ice and some possible solid phases of the binary salt $MgCl_2$ (namely $MgCl_2 \cdot 12H_2O$, $MgCl_2 \cdot 8H_2O$, and $MgCl_2 \cdot 6H_2O$). The thermodynamic model for the aqueous phase was the Pitzer model [33, 34] and the solid phases present were modeled by their re-
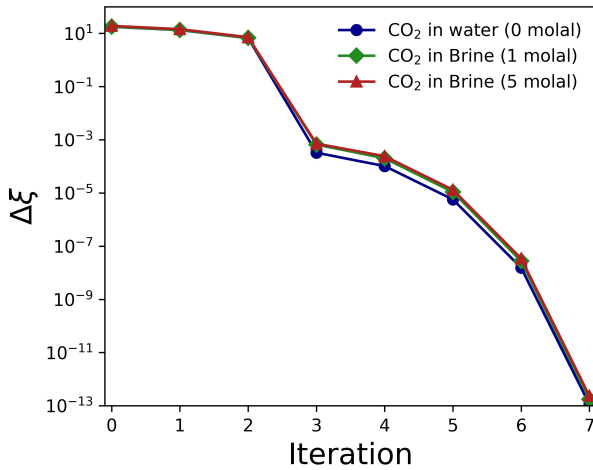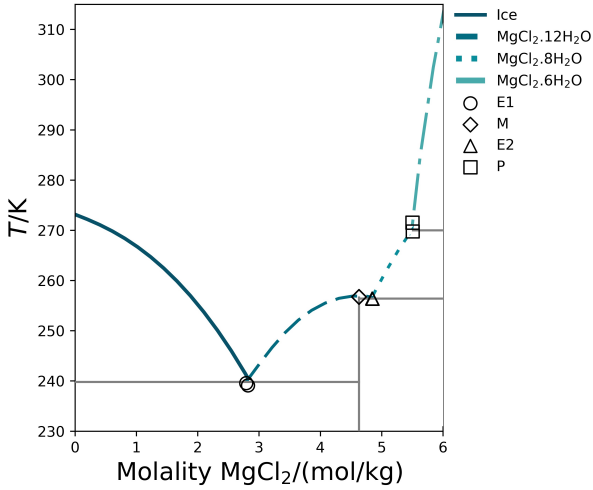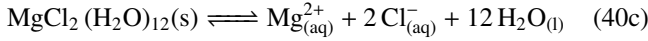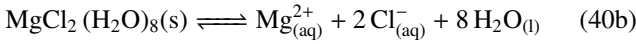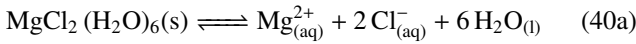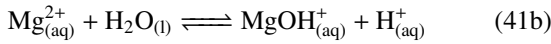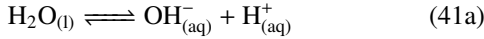
Figure 3: Solubilities of MgCl$_2$ hydrates and ice at 1 atm.

Figure 4: Convergence behavior of the saturation algorithm at points of the different phase boundary curves. Temperatures at which every phase was analyzed: 271.08K for ice, 256.58 K for MgCl$_2\cdot$12H$_2$O, 268.72 K for MgCl$_2\cdot$8H$_2$O, and 284.68 K for MgCl$_2\cdot$6H$_2$O.

action constants. The precipitation reactions considered were:

$$MgCl_2 (H_2O)_6(s) \rightleftharpoons Mg^{2+}_{(aq)} + 2\,Cl^-_{(aq)} + 6\,H_2O_{(l)} \quad (40a)$$

$$MgCl_2 (H_2O)_8(s) \rightleftharpoons Mg^{2+}_{(aq)} + 2\,Cl^-_{(aq)} + 8\,H_2O_{(l)} \quad (40b)$$

$$MgCl_2 (H_2O)_{12}(s) \rightleftharpoons Mg^{2+}_{(aq)} + 2\,Cl^-_{(aq)} + 12\,H_2O_{(l)} \quad (40c)$$

In addition to that, the speciation reactions in the aqueous phase were:

$$H_2O_{(l)} \rightleftharpoons OH^-_{(aq)} + H^+_{(aq)} \quad (41a)$$

$$Mg^{2+}_{(aq)} + H_2O_{(l)} \rightleftharpoons MgOH^+_{(aq)} + H^+_{(aq)} \quad (41b)$$

The parameters were taken from the Frezchem database [43] from PHREEQC [See supplementaty information]. The analysis of degrees of freedom shows that 4 elements are needed to model such a system and they were selected as H$^+$, OH$^-$, Mg^{2+} and Cl$^-$. Two phases were considered in all calculations, namely an aqueous phase containing electrolytes and a pure solid phase (one of the aforementioned solid hydrates or ice). Solid phases were the incipient ones ($\alpha^r_j = 0$) and all elements were present in the aqueous phase ($\alpha^r_{aq} = 1$). As in the previous example, the change in mole numbers of a phase because of the speciation reactions was negligible, and the element and mole amounts are virtually the same. The whole range of solubility was spanned by increasing the element amount of Mg^{2+} and Cl$^-$ following the stoichiometric of the binary MgCl$_2$ salt. The initial point had the following element specification $b_{H^+} = 55.51$ mol, $b_{OH^-} = 55.51$ mol, $b_{Mg^{2+}} = b_{Cl^-} = 0$ mol.

The results for the salt solubility problem are presented in Figure 3. The colored lines were obtained from the saturation point algorithm, and the solid gray lines were inferred from the calculated lines. The dots represent experimental points of the eutectic point of ice and MgCl$_2 \cdot$ 12H$_2$O (E1), of the congruent melting of MgCl$_2 \cdot$ 12H$_2$O (M), of the eutectic point of MgCl$_2 \cdot$ 12H$_2$O and MgCl$_2 \cdot$ 8H$_2$O (E2), and of the peritectic point involving MgCl$_2 \cdot$ 8H$_2$O and MgCl$_2 \cdot$ 6H$_2$O (P). Experimental data were taken from Linke and Seidell [44] and Steiger
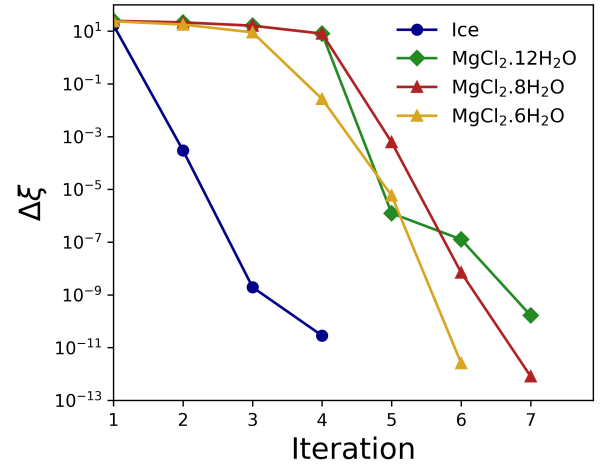
et al. [45] *apud* Li et al. [46]. The calculations agree with the experiments and the algorithm performed successfully throughout the whole range of compositions studied. Figure 4 shows the convergence behavior, by analyzing the maximum absolute value of any working variable ($\Delta\xi$) at a given iteration for one point in each of the four calculated curves. Second order convergence close to the solution can be observed for most of the curves. The derivatives of the aqueous model were obtained numerically.

3.3. PT Phase Envelope: Alkene Hydration Reaction

For all the phase diagrams presented in this work, PT phase envelopes under the influence of chemical reactions have been studied the least, especially when compared to their non-reactive counterparts. Research on phase envelope algorithms for non-reactive systems is a rather mature field and has covered a great number of aspects of the problem. One can find examples covering the core of the saturation algorithm [22], exploring strategies on envelope tracing [47], investigating different thermodynamic variables [48, 49], handling more than two-phases [50, 51], or including other physical effects in the problem [52, 53]. Meanwhile, phase envelope studies including chemical reactions are rather rare. Wilhelmsen et al.[54], in a recent review about thermodynamic modeling using EoS, stated that the numerically efficient plotting of phase envelopes of reactive mixtures remains an area under development. The authors also pointed out that robust and reliable algorithms involving chemical reactions are still required for advancing the thermodynamic modeling of reactive systems. The scarcity of works is especially intriguing when one considers the applications of reactive phase envelopes. The design of reactors at supercritical conditions, for instance, relies on the correct description of reactive phase behavior close to the critical point [55], and chemical reactions might alter significantly the phase split and critical conditions of certain systems [56, 57]. There are

(a) Specified α (b) Specified β^r
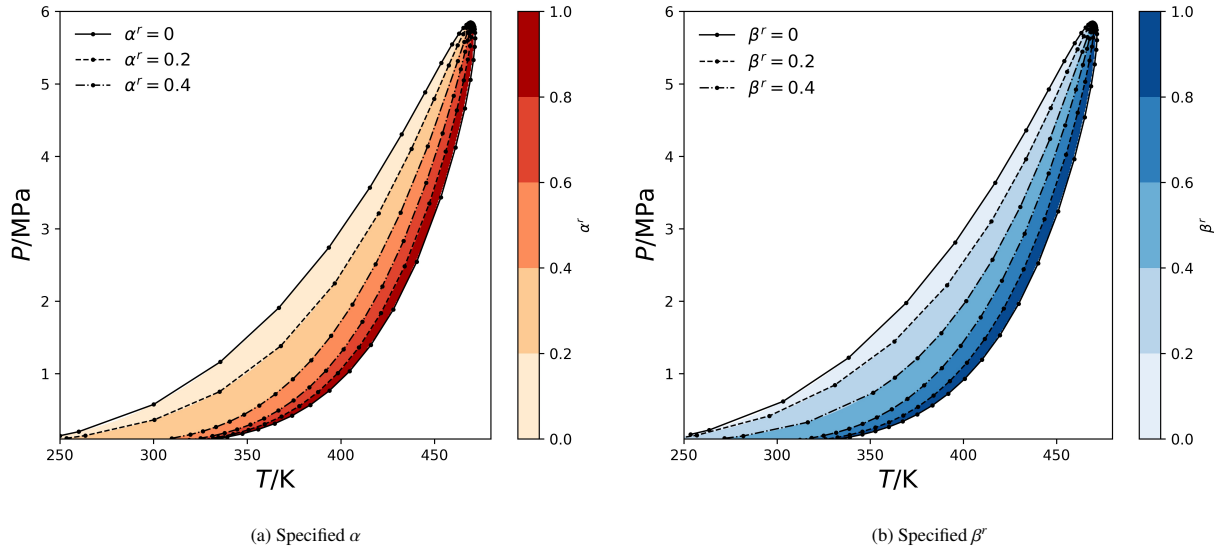
Figure 5: Phase envelope of the alkene hydration system at the initial load of 1, 1, 0 and 0.8 moles of propene, water, 1-propanol and propane, respectively. (a) Saturation and quality lines calculated using the saturation algorithm at fixed α compared to shaded values of α calculated using RAND. (b) Saturation and quality lines calculated using the saturation algorithm at fixed β^r compared to shaded values of β^r calculated using RAND.

(a) Specified α (b) Specified β^r
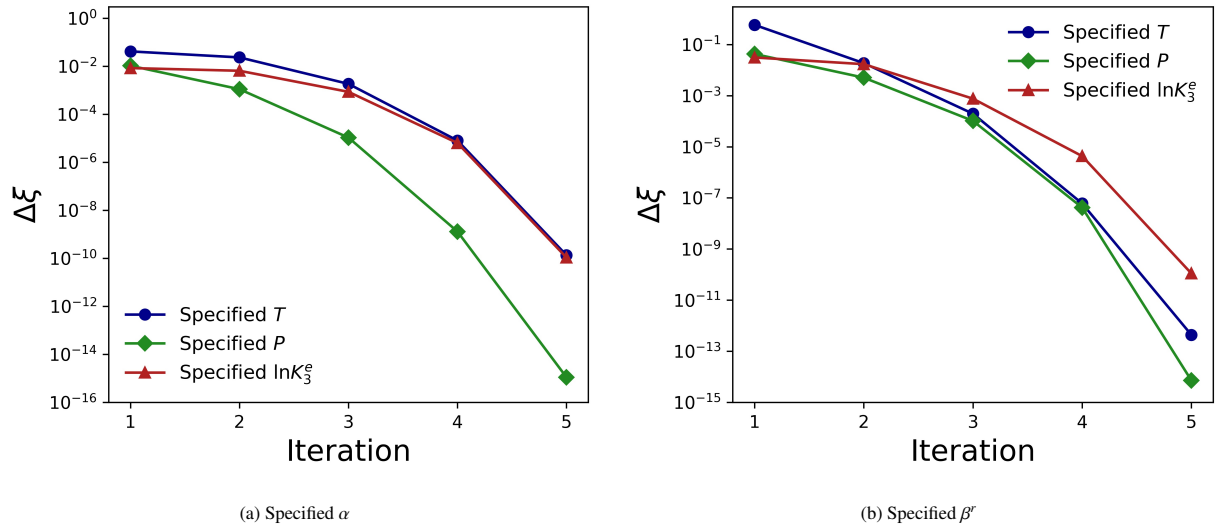
Figure 6: (a) Convergence behavior of the algorithm at fixed α at three different phase envelope specifications (T, P and $\ln K_3^e$ (propane)); (b) Convergence behavior of the algorithm at fixed β^r at three different phase envelope specifications (T, P and $\ln K_3^e$ (propane)).

works trying to understand the interplay between phase equilibrium and chemical reactions involving many different chemical processes such as biodiesel production [58] and thermal cracking of hydrocarbon fuels [59].

Here, we studied the phase diagram of the system propene, water and 1-propanol in the presence of the inert component propane. Similar systems have been studied before using of flash calculations [60, 61, 62, 16]. Propene and water react to form 1-propanol subject to the following stoichiometry:

$$H_2 O + C_3 H_6 \rightleftharpoons C_3 H_7 OH \tag{42}$$
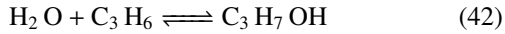
The system can be fully represented by 3 elements ($N_E = N_C - N_R = 4 - 1$). They were selected as actual species in the system: propene, water and propane. 1-propanol is considered to be a species formed by the elements propene and water. The reaction constant was fixed at the value of 23 at the ideal gas state and $P = 0.1013$ MPa [60, 61]. The mixture studied here was initially loaded with 1, 1, 0 and 0.8 moles of propene, water, 1-propanol and propane, respectively. Two different phase envelopes for this system are presented in Figure 5. In Figure 5 (a), we have calculated saturation lines at fixed values of α, i.e., using Equation 21 as specification, at 0, 0.56 and 1.12 (corresponding to 0, 0.2 and 0.4 in a normalized basis, α^r), and compared them to the α^r obtained from the RAND algorithm for flash calculations. We see that the calculated lines fall exactly at the border between shades, indicating that the saturation RAND agrees with the regular flash RAND algorithm. Figure 5 (b) shows a similar analysis, but with saturation lines calculated at fixed β^r, i.e., using Equation 22 as specification. Once again, we see that the saturation algorithm agrees with the regular CPE RAND. Throughout the phase envelope construction, the second specified variable (final row of Equation 16) changed according to the sensitivity vector. The convergence behavior of some of the points in the α^r and the β^r phase diagram at different specifications are presented in Figure 6 (a) and (b), respectively. We see that the algorithm presents second order convergence regardless of the specified variable selected.

Figure 7 compares the variations in $\ln K$ and $\ln K^e$ with temperature and pressure. In Figures 7 (a) and (b), we show the calculated values for the usual definition of $\ln K$ (component-based) as a function of temperature and pressure, respectively, throughout the phase envelope construction for incipient conditions ($\alpha^r = \beta^r = 0$). The mixture had the same initial loads as the ones used in Figure 5 (1, 1, 0 and 0.8 moles of propene, water, 1-propanol and propane). The definition of K_i in this case is

$$K_i = \frac{x_{i,1}}{x_{i,2}} \tag{43}$$

$x_{i,1}$ is a general expression for the mole fraction of component i in an incipient phase 1, and $x_{i,2}$ is a general expression for the mole fraction of component i in a bulk phase 2. The values obtained during bubble point calculations are represented as solid lines, whereas those obtained during dew point calculations are represented as dashed lines. The most notable feature of $\ln K_i$ for any component i is that it crosses the value of zero at the critical condition for all components simultaneously. That is where

the solid lines of bubble point calculations meet the dashed lines of dew point calculations, and the bulk phase in the calculation switches its phase state.

Light components, propene and propane, have positive values of $\ln K$ in the bubble points, that is, they are more abundant in the incipient vapor phase, than in the bulk liquid phase. After crossing the critical point, this tendency is inverted and light components have negative $\ln K$ in dew point calculations. This means that, in dew points calculations, they are less abundant in the incipient liquid phase, than in the bulk vapor phase. Heavy components, such as 1-propanol, have negative values of $\ln K$ in the bubble points, i.e., they are less abundant in the incipient vapor phase, than in the bulk liquid phase. Once the critical point is reached, this tendency is also inverted and $\ln K$ of heavy components becomes positive in dew point calculations, meaning that they are more abundant in the incipient liquid phase, than in the bulk vapor phase. Water, on the other hand, exhibits a peculiar behavior. Its value of $\ln K$ is negative throughout most of the range of T and P studied here. This indicates that water is almost always less abundant in the incipient phase than in the bulk phase, no matter whether it is a bubble point or a dew point.

In Figure 7 (c) and (d), we show the values of $\ln K^e$ during the phase envelope construction for the three elements defined here (propene, water and propane, whereas 1-propanol as a species is formed by the elements propene and water) as a function of temperature and pressure, respectively. $\ln K_k^e$ for a component k is defined by Equation 3.

From Figure 7 (c) and (d), we see that $\ln K^e$ retains the main feature of $\ln K$ for the development of saturation algorithms, which is the value of zero at the critical point. That is also the point where bubble point lines (solid lines) meet dew point lines (dashed lines). Here, the volatility interpretation is rather non-intuitive, as elements are arbitrarily assigned and do not possess individual values of critical temperatures or critical pressures that determine how light or heavy they are. Nevertheless, we can relate their behavior to Figures 7 (a) and (b). Element propane is just present in component propane (the light component), whereas elements propene and water are constituents of component 1-propanol (the heavy component). As such, element propane exhibits a behavior typical of light components in non-reactive systems. It has a positive $\ln K^e$ value in bubble point calculations and a negative $\ln K^e$ value in dew point calculations. The opposite is also true for elements water and propene, which have positive values of $\ln K^e$ in dew point calculations and negative values of $\ln K^e$ in bubble point calculations.

Furthermore, it should be noted that the quality lines at constant α^r (Figure 5 (a)) differ from the the quality lines at constant β^r (Figure 5 (b)). They become, however, close to each other as they approach the critical point. In Figure 8, we compare both quality lines (element quality lines and component quality lines). In this figure, red quality lines are the ones for β, whereas the ones for α are presented in black. The incipient lines ($\beta^r = 0$ and $\alpha^r = 0$) are the same in both paradigms. The quality lines, however, differ considerably at lower temperatures and pressures, but become similar as they approach the critical point. This can be explained by the phases becoming
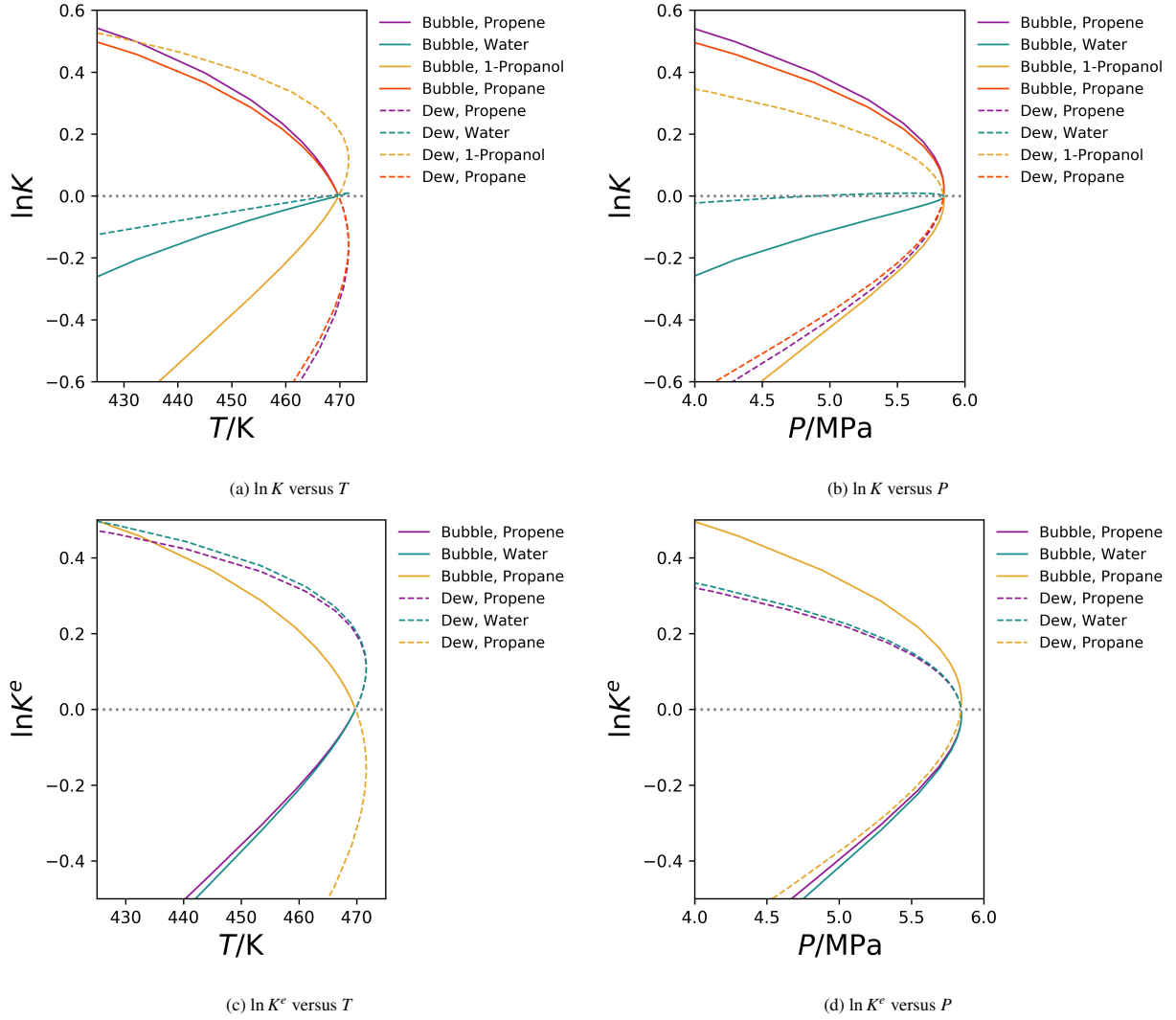
(a) $\ln K$ versus T

(b) $\ln K$ versus P

(c) $\ln K^e$ versus T

(d) $\ln K^e$ versus P

Figure 7: Comparison of $\ln K$ and $\ln K^e$ in the phase envelope (β^r and α^r set to zero): (a) $\ln K$ versus temperature; (b) $\ln K$ versus pressure; (c) $\ln K^e$ versus temperature; (d) $\ln K^e$ versus pressure.
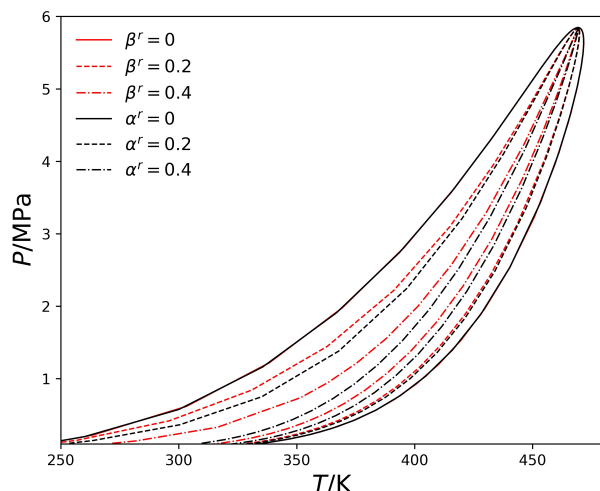
Figure 8: Comparison of phase envelopes of the alkene hydration with component-based quality lines (β) and with element-based quality lines (α).
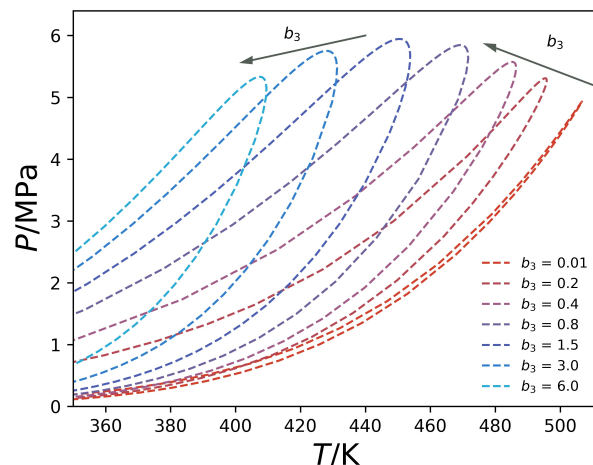

Figure 9: Phase envelopes of the reactive mixture of propene, water and 1-propanol at the initial mole numbers of 1, 1 and 0, respectively, with different amounts of the inert component propane (0.01, 0.2, 0.4, 0.8, 1.5, 3.0 and 6.0).

similar in their composition, both in terms of components (Figures 7 (a) and (b)) and in terms of elements (Figures 7 (c) and (d)).

Finally, the methodology presented here is a useful tool to understand the impact one of the components might have in the phase behavior of reactive mixtures. In Figure 9, we present several phase envelopes obtained by changing the amount of the inert component (propane) in the mixture (b_3). The initial amount of the other components was kept constant and the following initial amounts of propane were studied: 0.01, 0.2, 0.4, 0.8, 1.5, 3.0, and 6.0 moles. The mixture has a very narrow boiling region when propane is present at small amounts. Propane addition leads to a wider phase envelope and a shift in the critical point to lower temperatures and higher pressures. The maximum critical pressure occurs at around 1.5 moles of propane (around 6 MPa), after which more propane addition leads to lower critical pressures (5.5 MPa at 3.0 moles of propane, and 5 MPa at 6.0 moles of propane).

3.4. PT Phase Envelope: Non-Reactive Hydrocarbon Mixture

Finally, we address the non-reactive case by analyzing the phase behavior of a hydrocarbon mixture. The simplification of the RAND method to non-reactive mixtures [12] is proved to be a good and reliable alternative to other flash approaches (such as the Rachford-Rice [25] or the Gibbs energy Minimization paradigms [63]). The results we present here show that the non-reactive RAND paradigm can also encompass saturation problems. Most of the phase envelope research for non-reactive systems works within the Rachford-Rice framework. The possibility of a non-reactive saturation RAND is especially advantageous from an implementation point of view, since the same matrices and variables from the RAND non-reactive flash algorithm can be readily incorporated in a saturation one.

The hydrocarbon mixture presented here consisted of the following components: methane, ethane, propane, n-heptane and n-octane at mole numbers of 0.4, 0.1, 0.1, 0.2 and 0.2, respec-

tively. The SRK-EoS [64] was used and the parameters are presented in the supplementary material to this paper.

Figure 10 shows the phase envelope of the mixture with saturation lines calculated using the methodology presented here and shades representing the values of β^r obtained from the two-phase flash. The saturation lines fall exactly on the borders between the shades, showing that the non-reactive saturation methodology agrees with the flash results. The convergence behavior for some points using different specified variables is presented in Figure 11, which shows that the algorithm presented second order convergence regardless of the variable selected.

4. Conclusions

In this work, we developed the saturation RAND formulation for the β-specification problems, such as saturation point problems, for mixtures with simultaneous chemical and phase equilibrium. The saturation RAND formulation was obtained by modifying the recently developed RAND-based flash formulation for reactive mixtures. The saturation RAND formulation, using λ, β, T and P as working variables, provides a second order convergence scheme for efficient solution of the β-specification problems. The element-based phase fraction or the component-based phase fraction can be used for specifying the problem, and they lead to different specification equations and formulations. We further extend the single-point formulation to construction of the whole PT phase diagram, using a methodology suggested by Michelsen for non-reactive mixtures. To ensure that the calculation could cross the critical point smoothly, we introduced element-based partition coefficients K^e to be used as specification variables. K^e are similar to the component-based equilibrium factors K-factors, and equal to 1 at the critical point. The phase envelope algorithm using the saturation RAND formulation represents a general solution to the β-specification problems for reactive mixtures, and can
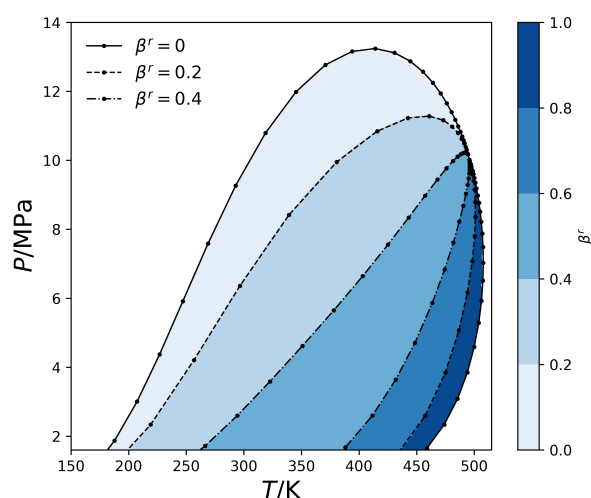
Figure 10: Phase envelope of the hydrocarbon mixture containing methane, ethane, propane, n-heptane and n-octane at 0.4, 0.1, 0.1, 0.2 and 0.2 moles, respectively. Saturation and quality lines calculated using the saturation algorithm at fixed β^r compared to shaded values of β^r calculated using the two-phase flash.

therefore be reduced to the special case for non-reactive mixtures. We showed how the reduced algorithm provides an alternative approach to Michelsen's phase envelope algorithm for non-reactive mixtures.

This new methodology was tested with four examples involving both VLE and SLE, utilizing both the $\gamma - \phi$ and $\phi - \phi$ approaches. The algorithm was tested to calculate the conditions in which incipient phases appear, resulting in the *Pxy* and *Txy* phase diagrams of Sections 3.1 and 3.2. The automatic construction of complete phase envelopes was presented in Section 3.3 for a system involving an alkene hydration reaction, where we also calculated both saturation lines and quality lines under two differen specifications, α and β^r. The final set of results showed the applicability of the method to non-reactive mixtures (Section 3.4). The algorithm showed second order convergence in all test examples and proved to be a versatile and reliable tool for phase diagram construction.

Our study suggests that robust and efficient phase equilibrium calculation algorithms, not limited to flash, can be developed for systems with complex chemical equilibria. The advancements reported here can find applications in several areas where the interplay between chemical reactions and phase behavior plays a major role, and this is not limited to VLE or SLE or any modeling strategy. In particular, the developments contribute directly to the PT phase envelope calculation where the studies for reactive systems are still rare.

References

[1] W. R. Smith, R. W. Missen, Chemical Reaction Equilibrium Analysis, Wiley, 1982.

[2] Y. A. Chang, S. Chen, F. Zhang, X. Yan, F. Xie, R. Schmid-Fetzer, W. A. Oates, Phase diagram calculation: Past, present and future, Progress in Materials Science 49 (2004) 313–345. doi:10.1016/S0079-6425(03)00025-2.

[3] G. M. Anderson, Thermodynamics of natural systems, second edition, 2nd ed., Cambridge University Press, New York, 2005. doi:10.1017/CBO9780511840258.

[4] T. Gasparik, Phase Diagrams for Geoscientists, 2nd ed., Springer US, New York, 2014.

[5] M. L. Michelsen, Phase equilibrium calculations. What is easy and what is difficult?, Computers and Chemical Engineering 17 (1993) 431–439. doi:10.1016/0098-1354(93)80034-K.

[6] E. H. Chimowltz, S. Macchietto, T. F. Anderson, L. F. Stutzman, Local Models for Representing Phase Equilibria in Multicomponent Nonideal Vapor-Liquid and Liquid-Liquid Systems. 3. Parameter Estimation and Update, Industrial and Engineering Chemistry Process Design and Development 25 (1986) 674–682. doi:10.1021/i200034a013.

[7] D. A. Berry, K. M. Ng, Synthesis of Reactive Crystallization Processes, AIChE Journal 43 (1997) 1737–1750. doi:10.1002/aic.690430711.

[8] C. S. Agger, H. Sørensen, Algorithm for Constructing Complete Asphaltene PT and Px Phase Diagrams, Industrial and Engineering Chemistry Research 57 (2018) 392–400. doi:10.1021/acs.iecr.7b04246.

[9] S. R. Brinkley, Calculation of the equilibrium composition of systems of many constituents, The Journal of Chemical Physics 15 (1947) 107–110. doi:10.1063/1.1746420.

[10] W. B. White, S. M. Johnson, G. B. Dantzig, Chemical equilibrium in complex mixtures, The Journal of Chemical Physics 28 (1958) 751–755. doi:10.1063/1.1732424.

[11] H. Greiner, An efficient implementation of newton's method for complex nonideal chemical equilibria, Computers and Chemical Engineering 15 (1991) 115–123. doi:10.1016/0098-1354(91)87010-7.

[12] D. Paterson, M. L. Michelsen, E. H. Stenby, W. Yan, New formulations for isothermal multiphase flash, Society of Petroleum Engi-
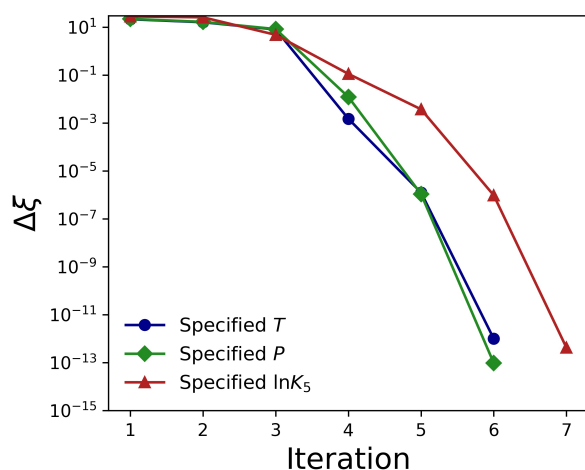
Figure 11: Convergence behavior of the non-reactive algorithm at fixed β^r at three different phase envelope specifications (T, P and $\ln K_5$ (n-octane)).

neers - SPE Reservoir Simulation Conference 2017 (2017) 1947–1964. doi:10.2118/182706-pa.

[13] D. Paterson, W. Yan, M. L. Michelsen, E. H. Stenby, Multiphase isenthalpic flash: General approach and its adaptation to thermal recovery of heavy oil, AIChE Journal 65 (2019) 281–293. doi:10.1002/aic.16371.

[14] C. Tsanas, E. H. Stenby, W. Yan, Calculation of multiphase chemical equilibrium in electrolyte solutions with nonstoichiometric methods, Fluid Phase Equilibria 482 (2019) 81–98. doi:10.1016/j.fluid.2018.10.008.

[15] D. Paterson, M. L. Michelsen, W. Yan, E. H. Stenby, Extension of modified RAND to multiphase flash specifications based on state functions other than (T,P), Fluid Phase Equilibria 458 (2018) 288–299. doi:10.1016/j.fluid.2017.10.019.

[16] F. d. A. Medeiros, E. H. Stenby, W. Yan, State function-based flash specifications for open systems in the absence or presence of chemical reactions, AIChE Journal 67 (2021). doi:10.1002/aic.17050.

[17] Z. K. Liu, First-principles calculations and CALPHAD modeling of thermodynamics, Journal of Phase Equilibria and Diffusion 30 (2009) 517–534. doi:10.1007/s11669-009-9570-6.

[18] S. Ung, M. F. Doherty, Theory of phase equilibria in multireaction systems, Chemical Engineering Science 50 (1995) 3201–3216. doi:10.1016/0009-2509(95)00159-3.

[19] S. Ung, M. F. Doherty, Vapor-liquid phase equilibrium in systems with multiple simultaneous chemical reactions, Chemical Engineering Science 50 (1995) 23–48. doi:10.1016/0009-2509(94)00180-Y.

[20] D. W. Slaughter, M. F. Doherty, Calculation of solid-liquid equilibrium and crystallization paths for melt crystallization processes, Chemical Engineering Science 50 (1995) 1679–1694. doi:10.1016/0009-2509(95)00010-3.

[21] M. L. Michelsen, Saturation point calculations, Fluid Phase Equilibria 23 (1985) 181–192. doi:10.1016/0378-3812(85)90005-6.

[22] M. L. Michelsen, Calculation of phase envelopes and critical points for multicomponent mixtures, Fluid Phase Equilibria 4 (1980) 1–10. doi:10.1016/0378-3812(80)80001-X.

[23] M. L. Michelsen, J. M. Mollerup, Thermodynamic Models: Fundamentals & Computational Aspects, 2nd ed. ed., Tie-Line Publications, Holte, Denmark, 2008.

[24] D. Paterson, Flash Computation and EoS Modelling for Compositional Thermal Simulation of Flow in Porous Media, Springer Theses, Springer International Publishing, 2019. doi:10.1007/978-3-030-11787-0.

[25] H. Rachford, J. Rice, Procedure for Use of Electronic Digital Computers in Calculating Flash Vaporization Hydrocarbon Equilibrium, Journal of Petroleum Technology 4 (1952) 19–3. doi:10.2118/952327-g.

[26] W. Yan, S. Huang, E. H. Stenby, Measurement and modeling of CO2 solubility in NaCl brine and CO2-saturated NaCl brine density, International Journal of Greenhouse Gas Control 5 (2011) 1460–1477. doi:10.1016/j.ijggc.2011.08.004.

[27] A. Venkatraman, L. W. Lake, R. T. Johns, Modelling the impact of geochemical reactions on hydrocarbon phase behavior during CO2 gas injection for enhanced oil recovery, Fluid Phase Equilibria 402 (2015) 56–68. doi:10.1016/j.fluid.2015.05.028.

[28] D. Barbosa, M. F. Doherty, The influence of equilibrium chemical reactions on vapor-liquid phase diagrams, Chemical Engineering Science 43 (1988) 529–540. doi:10.1016/0009-2509(88)87014-3.

[29] S. K. Wasylkiewicz, S. Ung, Global phase stability analysis for heterogeneous reactive mixtures and calculation of reactive liquid-liquid and vapor-liquid-liquid equilibria, Fluid Phase Equilibria 175 (2000) 253–272. doi:10.1016/S0378-3812(00)00451-9.

[30] A. Bonilla-Petriciolet, U. I. Bravo-Sánchez, F. Castillo-Borja, S. Frausto-Hernández, J. G. Segovia-Hernández, Gibbs energy minimization using simulated annealing for two-phase equilibrium calculations in reactive systems, Chemical and Biochemical Engineering Quarterly 22 (2008) 285–298.

[31] M. H. Reis, L. F. Mascolo, M. R. Wolf-Maciel, Development of a robust algorithm to compute reactive azeotropes, Brazilian Journal of Chemical Engineering 23 (2006) 395–403. doi:10.1590/S0104-66322006000300013.

[32] E. S. Pérez Cisneros, R. Gani, M. L. Michelsen, Reactive separation systems - I. Computation of physical and chemical equilibrium, Chemical Engineering Science 52 (1997) 527–543. doi:10.1016/S0009-2509(96)00424-1.

[33] K. S. Pitzer, Thermodytriarnics of Electrolytes. I. Theoretical Basis and General Equations, The Journal of Physical Chemistry 77 (1973) 268–277. doi:10.1021/j100621a026.

[34] A. R. Felmy, J. H. Weare, The prediction of borate mineral equilibria in natural waters: Application to Searles Lake, California, Geochimica et Cosmochimica Acta 50 (1986) 2771–2783. doi:10.1016/0016-7037(86)90226-7.

[35] D.-Y. Peng, D. B. Robinson, A New Two-Constant Equation of State, Industrial & Engineering Chemistry Fundamentals 15 (1976) 59–64. doi:10.1021/i160057a011.

[36] D. L. Parkhurst, C. A. J. Appelo, Description of input and examples for PHREEQC version 3: a computer program for speciation, batch-reaction, one-dimensional transport, and inverse geochemical calculations, Technical Report, Reston, VA, 2013. doi:10.3133/tm6A43.

[37] A. V. García, K. Thomsen, E. H. Stenby, Prediction of mineral scale formation in geothermal and oilfield operations using the extended UNIQUAC model. Part I. Sulfate scaling minerals, Geothermics 34 (2005) 61–97. doi:10.1016/j.geothermics.2004.11.002.

[38] M. A. McDonald, H. Salami, P. R. Harris, C. E. Lagerman, X. Yang, A. S. Bommarius, M. A. Grover, R. W. Rousseau, Reactive crystallization: a review, Reaction Chemistry & Engineering (2021). doi:10.1039/d0re00272k.

[39] R. Z. Cui, S. H. Sang, W. Li, Y. P. Dong, (Solid + Liquid) Phase Equilibria in the Quaternary System (NaBr + MgBr2 + CaBr2 + H2O) at 298.15 K, Journal of Chemical and Engineering Data 63 (2018) 3400–3407. doi:10.1021/acs.jced.8b00291.

[40] M. Teles dos Santos, V. Gerbaud, G. A. Roux, Modeling and simulation of melting curves and chemical interesterification of binary blends of vegetable oils, Chemical Engineering Science 87 (2013) 14–22. doi:10.1016/j.ces.2012.09.026.

[41] N. D. Carareto, T. Castagnaro, M. C. Costa, A. J. Meirelles, The binary (solid + liquid) phase diagrams of (caprylic or capric acid) + (1-octanol or 1-decanol), Journal of Chemical Thermodynamics 78 (2014) 99–108. doi:10.1016/j.jct.2014.06.011.

[42] K. Tamura, T. Kasuga, T. Nakagawa, Phase behavior and solid–liquid equilibria of aliphatic and aromatic carboxylic acid mixtures, Fluid Phase Equilibria 420 (2016) 24–29. doi:10.1016/j.fluid.2015.12.021.

[43] G. M. Marion, M. V. Mironenko, M. W. Roberts, FREZCHEM: A geochemical model for cold aqueous solutions, Computers and Geosciences 36 (2010) 10–15. doi:10.1016/j.cageo.2009.06.004.

[44] W. F. Linke, A. Seidell, Solubilities: Inorganic and Meta-Organic Compounds, 4th ed., American Chemical Society, Washington, D. C., 1965.

[45] M. Steiger, K. Linnow, D. Ehrhardt, M. Rohde, Decomposition reactions of magnesium sulfate hydrates and phase equilibria in the MgSO4-H2O and Na+ - Mg 2+ - Cl- - H2O systems with implications for Mars, Geochimica et Cosmochimica Acta 12 (2011) 3600–3626.

[46] D. Li, D. Zeng, X. Yin, H. Han, L. Guo, Y. Yao, Phase diagrams and thermochemical modeling of salt lake brine systems. II. NaCl+H2O, KCl+H2O, MgCl2+H2O and CaCl2+H2O systems, Calphad: Computer Coupling of Phase Diagrams and Thermochemistry 53 (2016) 78–89. doi:10.1016/j.calphad.2016.03.007.

[47] I. K. Nikolaidis, G. C. Boulougouris, L. D. Peristeras, I. G. Economou, Construction of phase envelopes for binary and multicomponent mixtures with Euler-Newton predictor-corrector methods, Fluid Phase Equilibria 505 (2020) 112338. doi:10.1016/j.fluid.2019.112338.

[48] D. V. Nichita, Density-based phase envelope construction, Fluid Phase Equilibria 478 (2018) 100–113. doi:10.1016/j.fluid.2018.09.007.

[49] D. V. Nichita, A simple approximate density-based phase envelope construction method, Fluid Phase Equilibria 499 (2019) 112245. doi:10.1016/j.fluid.2019.112245.

[50] N. Lindeloff, M. L. Michelsen, Phase Envelope Calculations for Hydrocarbon-Water Mixtures, Proceedings - SPE Annual Technical Conference and Exhibition (2002) 3749–3756. doi:10.2118/77770-ms.

[51] M. Cismondi, Phase Envelopes for Reservoir Fluids with Asphaltene Onset Lines: An Integral Computation Strategy for Complex Combinations of Two- and Three-Phase Behaviors, Energy and Fuels 32 (2018) 2742–2748. doi:10.1021/acs.energyfuels.7b02790.

[52] D. R. Sandoval, M. L. Michelsen, W. Yan, E. H. Stenby, VT-Based Phase Envelope and Flash Calculations in the Presence of Capillary Pressure, Industrial and Engineering Chemistry Research 58 (2019) 5291–5300. doi:10.1021/acs.iecr.8b05976.

[53] D. V. Nichita, Density-based phase envelope construction including capillary pressure, Fluid Phase Equilibria 498 (2019) 33–44. doi:10.1016/j.fluid.2019.06.018.

[54] Ø. Wilhelmsen, A. Aasen, G. Skaugen, P. Aursand, A. Austegard, E. Aursand, M. A. Gjennestad, H. Lund, G. Linga, M. Hammer, Thermodynamic Modeling with Equations of State: Present Challenges with Established Methods, Industrial and Engineering Chemistry Research 56 (2017) 3503–3515. doi:10.1021/acs.iecr.7b00317.

[55] E. Brignole, S. Pereda, Phase equilibrium engineering principles in reactive systems, volume 3, 2013. doi:10.1016/B978-0-444-56364-4.00011-X.

[56] M. Nunes da Ponte, Phase equilibrium-controlled chemical reaction kinetics in high pressure carbon dioxide, Journal of Supercritical Fluids 47 (2009) 344–350. doi:10.1016/j.supflu.2008.10.007.

[57] J. Ke, H. Buxing, M. W. George, H. Yan, M. Poliakoff, How does the critical point change during a chemical reaction in supercritical fluids? A study of the hydroformylation of propene in supercritical CO2, Journal of the American Chemical Society 123 (2001) 3661–3670. doi:10.1021/ja003446o.

[58] A. A. Albuquerque, F. T. Ng, L. Danielski, L. Stragevitch, Phase equilibrium modeling in biodiesel production by reactive distillation, Fuel 271 (2020) 117688. doi:10.1016/j.fuel.2020.117688.

[59] R. Jiang, G. Liu, Z. You, M. Luo, X. Wang, L. Wang, X. Zhang, On the critical points of thermally cracked hydrocarbon fuels under high pressure, Industrial and Engineering Chemistry Research 50 (2011) 9456–9465. doi:10.1021/ie200885p.

[60] R. P. Stateva, W. A. Wakeham, Phase Equilibrium Calculations for Chemically Reacting Systems, Industrial and Engineering Chemistry Research 36 (1997) 5474–5482. doi:10.1021/ie9702643.

[61] A. Bonilla-Petriciolet, A. Acosta-Martínez, U. I. Bravo-Sánchez, J. G. Segóvia-Hernández, Formulation of new conditions for bubble and dew point calculations in multireactive mixtures, Chemical and Biochemical Engineering Quarterly 20 (2006) 111–118.

[62] C. Tsanas, E. H. Stenby, W. Yan, Calculation of Multiphase Chemical Equilibrium by the Modified RAND Method, Industrial and Engineering Chemistry Research 56 (2017) 11983–11995. doi:10.1021/acs.iecr.7b02714.

[63] M. L. Michelsen, The isothermal flash problem. Part II. Phase-split calculation, Fluid Phase Equilibria 9 (1982) 21–40. doi:10.1016/0378-3812(82)85002-4.

[64] G. Soave, Equilibrium constants from a modified Redlich-Kwong equation of state, Chemical Engineering Science 27 (1972) 1197–1203. doi:10.1016/0009-2509(72)80096-4.